CELIDON: Supporting First Responders through 3D AOA-based UWB Ad-Hoc Localization

Janis Tiemann, Oliver Fuhr and Christian Wietfeld
TU Dortmund University, Communication Networks Institute (CNI)
Otto-Hahn-Str. 6, 44227 Dortmund, Germany
{janis.tiemann, oliver.fuhr, christian.wietfeld}@tu-dortmund.de

***Abstract*—For many applications relative position information is critical. One particular case is the prevention of compressed air breathing accidents in operations with low visibility. Here, separation of first responders in an unknown and dangerous environment could yield a fatal outcome. The goal of this work is to introduce technology that assists firefighters in situations with no visibility to locate team members. Due to the lack of pre-installed infrastructure, a relative ad-hoc localization scheme without the need for in place infrastructure is required. We propose a three-dimensional ultra-wideband based scheme and show a functional prototype with integrated transceivers combining both, two-way ranging range finding and phase-difference of arrival direction finding. Further, we show a potential architecture for integration in firefighter equipment such as helmet and mask utilizing augmented reality technology. Through multiple experiments we could show, that in the given laboratory setup direction estimation with an accuracy of 20° and position finding with an accuracy of 30 cm is possible with the proposed approach.**

***Index Terms*—Ultra-wideband (UWB), Wireless Positioning, Angle of Arrival (AOA), Phase-Difference of Arrival (PDOA), Infrastructure-Free, Infrastructure-Less, Ad-Hoc Localization, First Responders, Firefighters, Low Visibility.**

I. Introduction and Related Work

Firefighters are often exposed to extreme conditions during operations. Orientation is particularly difficult when there is a lot of smoke inside buildings, which means that the firefighters can be separated from each other. Those separations can lead to compressed air breathing apparatus accidents, which in some cases can have fatal outcomes. Generally, those accidents are being avoid by tactics. Nevertheless, there are cases where separation cannot be avoided. The primary goal of this work is to prevent critical compressed air breathing apparatus accidents of firefighters by making them ”visible” to the rescue teams as illustrated in Fig. 1. There are several ways of localization indoors. One of the most recent as emerging in many phones and tablets is optical simultaneous localization and mapping (SLAM) methods such as [1]. However, they are utilizing camera pictures [2] or structured light are not applicable in low visibility. Pedestrian dead reckoning (PDR), the integration of inertial measurement unit (IMU) data is prone to accumulating large errors over time, see [3], [4]. Radar-based SLAM such as [5] is a promising candidate, but features uncertainty and does not provide direct identification and direct relative localization of nodes. Therefore, our approach is developing a wireless localization for the orientation of firefighters in environments with low visibility based on

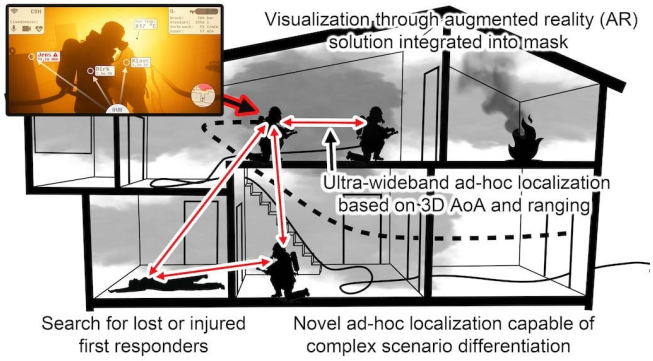

Fig. 1. Illustration of the low-visibility scenario in which the proposed ad-hoc localization approach provides a significant benefit by enabling the firefighters to find separated first responders or persons in distress.

ultra-wideband (UWB) communication and augmented reality (AR) technology. The majority of UWB localization is based on static infrastructure tracking or providing anchors for the moving nodes, see [6]–[11]. Other promising approaches track participants based on the channel impulse response in the UWB signal, see [12]. However, placing static infrastructure pre-operation is not possible in real-world operations, where every second counts.

Due to this, we propose using no infrastructure at all and combining 3D angle of arrival (AOA) estimation with two-way ranging (TWR) to achieve relative ad-hoc localization. Recent work on 2D AOA estimation using integrated transceiver hardware showed that this could be achieved with promising accuracy, see [13], [14]. Further, the newest generation of phones from leading manufacturers integrates UWB transceivers and is capable of 2D direction finding, see [15]. In [16] a single-anchor method is proposed to estimate the 2D angle of arrival using the channel impulse responses on multiple UWB transceivers and an array of three antennas in a triangle formation. Through this, the authors could achieve a 360° field of view in 2D ad-hoc localization utilizing ranges and AOAs. Similar approaches with simultaneous or concurrent ranging but without phase-based AOA estimation have been proposed by [17], [18]. For key-fob applications such as [19], those approaches might be utilized to estimate the location of a person entering a vehicle given the potentially large spatial spread of nodes in a vehicle. For application of first responders though, this spread is insufficient. This is why this work

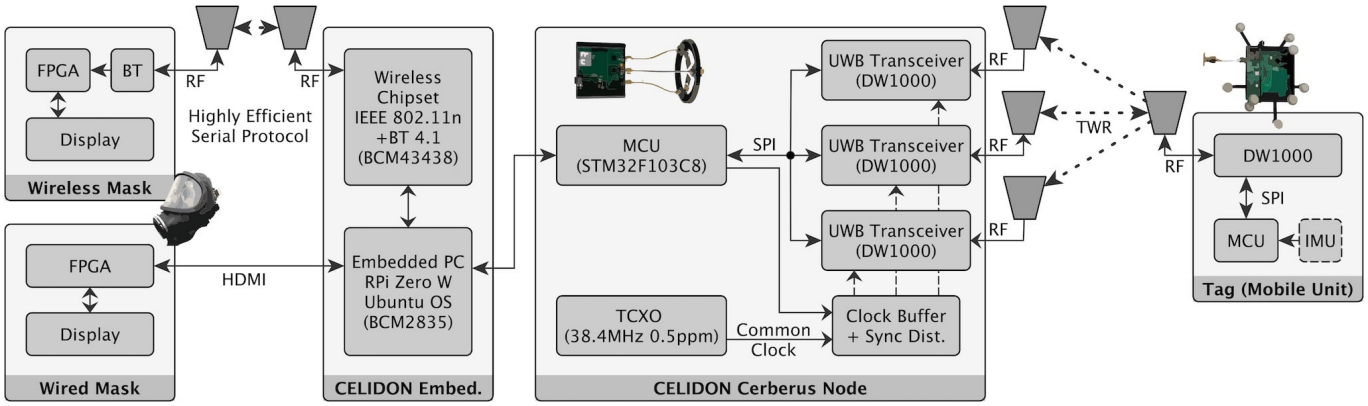

Fig. 2. Schematic illustration of the system architecture for the proposed integrated ad-hoc localization system. At the center is the *CELIDON Cerberus* ad-hoc localization node, capable of tracking mobile units or other active ad-hoc localization nodes, depicted in the right. When connected to an embedded PC, it is enabled to provide a visualization for the rescue forces within a wired or wirelessly connected mask, depicted on the left.

proposes 3D ad-hoc localization based on phase-difference based AOA estimation. Here, the antennas are separated with roughly half of the carrier frequency wave length. Due to this, future integration in the clothing of first responders is possible. However, 3D direction finding with IEEE 802.15.4a compatible UWB transceiver chipsets has, best to the authors knowledge, not been integrated and evaluated experimentally. This work aims to provide a first proof of concept experimental evaluation of such a 3D ad-hoc localization solution.

II. Proposed Ad-Hoc Localization Approach

This work proposes a 3D capable ad-hoc localization scheme for the support of first responders. The proposed concept is based on simultaneous ranging and angle of arrival (AOA) estimation. To illustrate the principle and the flow of information, the overall system topology is depicted in Fig. 2. The *CELIDON Cerberus* node, detailed in Fig. 3 is equipped with multiple transceivers from which one is actively conducting two-way ranging (TWR) with mobile units. These mobile units can be simple and small battery operated nodes or other *CELIDON Cerberus* nodes. The other transceivers are evaluating the signal passively. In order to achieve a common timebase, all transceivers are fed with medium quality temperature controlled crystal oscillator (TCXO) which is then distributed through a clock buffer with very low jitter.

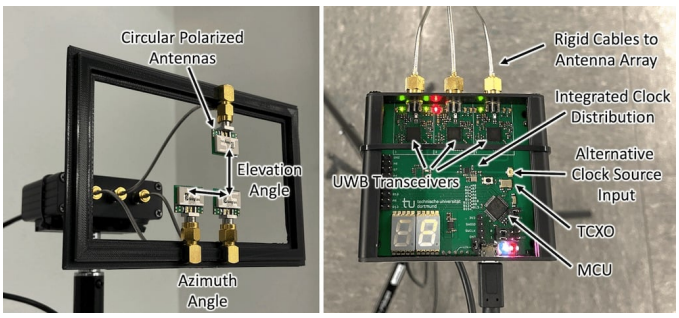

Fig. 3. Pictures of the *CELIDON Cerberus* antenna constellation and evaluation hardware for the proposed 3D ad-hoc localization concept.

All transceivers are interfaced using an ARM microcontroller unit (MCU). After processing, the obtained ranges and angles are then sent to an embedded computer which is capable of recording, communicating and provisioning of a rendered graphical user interface (GUI) for the rescue forces. The rendered GUI can then be displayed over HDMI on a heads up display (HUD) in a wired mask, or is transmitted wirelessly over a highly efficient serial protocol utilizing Bluetooth Low Energy (BLE). In this case, the rendering is conducted on the mask itself.

A. Physical Layer Channel Access

The ranging is conducted using symmetric double-sided two-way ranging (SDS-TWR), a time of arrival (TOA)-based method to obtain a distance between two UWB nodes. Here, the symmetric reply times are used to cancel the clock-drift induced error. There are other concepts utilizing alternative methods to cancel these errors, for example two-way ranging with multiple acknowledgments (TWR-MA) which utilizes repetition of frames in order to estimate clock drift, see [20]. It is expected that in future standards [21], succeeding [22], reply times are reduced to a degree that these errors become negligible, see [23]. The parameters of the physical layer configuration are listed in Tab. I.

B. Phase-Difference of Arrival (PDOA) estimation

In order to obtain the angle of arrival (AOA) of an arriving signal, the *CELIDON Cerberus* utilizes it's three transceiver heads. The method is based on [13] and the underlying 2D-capable hardware was used as a reference for the implementation of the hardware developed in the course of this work. At each transceiver n, the phase Φ_n of the received channel

TABLE I
Channel configuration used in the experiments.

f_c [GHz]	B [MHz]	n_{prc}	f_{pr} [MHz]	R [Mbps]	c_{pr}	n_{pr}
6.4896	499.2	127	62.4	6.8	9	256

impulse response (CIR) is evaluated, see (1). Here, the *I/Q* samples of the correlation with a reference signal are sampled in an accumulator register. The register is evaluated on the position of the detected first path t_{fp}.

$$\Phi_n = arg(I_n(t_{fp}) + i \cdot Q_n(t_{fp})) \tag{1}$$

Due to the coarse sampling interval of roughly 1 ns, a phase correction coefficient β_n is utilized to correct each Φ_n. The phase difference of arrival (PDOA) $\alpha_{n,k}$ is then obtained as the difference between the individual phases of the transceiver nodes n and k, see (2).

$$\alpha_{n,k} = \Phi_n - \Phi_k - (\beta_n - \beta_k) \tag{2}$$

The basic principle of the scheme is depicted in Fig. 4. Here, an experimentally recorded channel impulse response is utilized to illustrate the resolution available to this approach.

C. Antenna Characteristics and Constellation

The achievable accuracy is mainly depending on the characteristics of the antennas and their constellation used for the PDOA measurements. Therefore, selection of the right antennas and antenna constellation for the design is critical. Due to the ad-hoc nature of localization, which implies frequent position and orientation changes, we chose circular polarized antennas as the basis for the proposed system. We utilize early samples of *Taoglas UWBCCP.01* antennas and integrate them on a custom break-out to evaluate different antenna constellations. An early comparison of the input return loss of the integrated breakout against printed circuit board prototypes for the *DWM1003* illustrates the good fit for IEEE 802.15.4a-2015 channel 5, see Fig. 5.

D. Compensation and Filtering

To achieve better PDOA estimation, two correction functions are applied to the angle estimation in order to compensate constellation-specific effects in the measurements. For the azimuth angle $\alpha_{az,pdoa}$, measurement is segmented into two segments depending on the sign of $\alpha_{0,2}$, see (3).

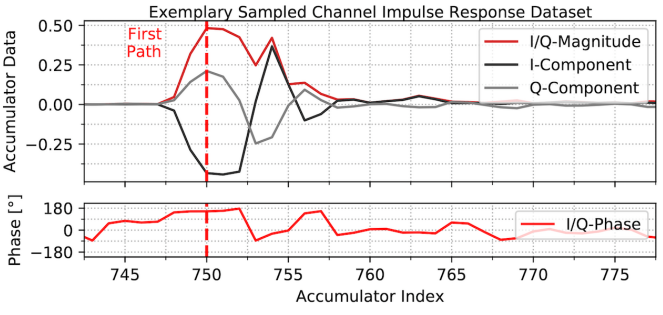

Fig. 4. Illustration of the phase measurement method at each transceiver n utilizing an experimentally captured channel impulse response (CIR). Note that the extracted *I/Q* phase Φ_n is corrected with an additional phase adjustment coefficient β_n.

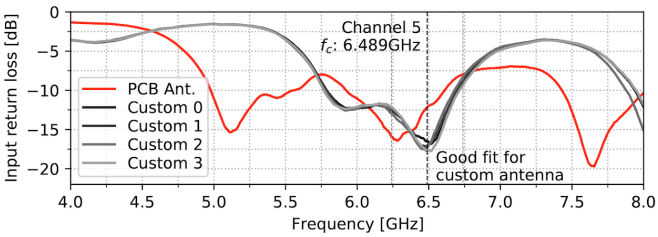

Fig. 5. Experimental analysis of the antenna input return loss on the custom breakout designed for antenna-placement evaluation compared to a PCB-based antenna design. To verify reproducibility, all four breakouts used in the following experimental evaluation were analyzed.

$$\alpha_{az,pdoa} = \begin{cases} 3/4 \cdot \alpha_{0,2} & \alpha_{0,2} \geq 0 \\ 5/4 \cdot \alpha_{0,2} & \alpha_{0,2} < 0 \end{cases} \tag{3}$$

For the elevation angle $\alpha_{el,pdoa}$, the readings are constrained in magnitude if the $\alpha_{0,2}$ is larger than $\pi/4$ to avoid outliers in the corners, see (4).

$$\alpha_{el,pdoa} = \begin{cases} 1/4 \cdot \alpha_{1,2} & |\alpha_{0,2}| \geq \pi/4 \\ \alpha_{1,2} & |\alpha_{0,2}| < \pi/4 \end{cases} \tag{4}$$

To smooth the results and provide more consistent feedback to the rescue forces, a filter is applied to the individual readings after compensation. The angular PDOA readings $\alpha_{az,pdoa}$ and $\alpha_{el,pdoa}$ are converted to complex unit vectors to support continuous filtering even when the angle changes from 180° to −180°.

A two-dimensional constant velocity Kalman filter as of [24] is utilized to track the individual components of the unit vector for each angle. For the angular components a measurement noise of $\sigma^2_{R,\alpha} = 5 \times 10^{-5}\,\text{rad}^2$ is assumed as well as a process noise of $\sigma^2_{Q,\alpha} = 0.5\,\text{rad}^2$. Similarly, the distance is filtered utilizing a one-dimensional constant velocity filter with a measurement noise of $\sigma^2_{R,d} = 0.05\,\text{m}^2$ and a process noise of $\sigma^2_{Q,\alpha} = 0.5\,\text{m}^2$.

Further, the resulting PDOA angles are converted to AOA angles as proposed in [13] to obtain better results with higher angles of incident, see (5).

$$\alpha_{az} = 1/0.95 \cdot \arcsin(\alpha_{az,pdoa}/\pi) \tag{5}$$

$$\alpha_{el} = 1/0.95 \cdot \arcsin(\alpha_{el,pdoa}/\pi) \tag{6}$$

Depending on the antenna characteristics and constellation the above mentioned parameters, especially for compensation might change in future integration of the proposed system.

E. Visualization

In order to provide a benefit in real missions, the key information needs to depicted in an intuitive form to the rescue forces. An early functional prototype is depicted in Fig. 6. The rendered visualization is integrated in a second step into a miniature heads-up display.

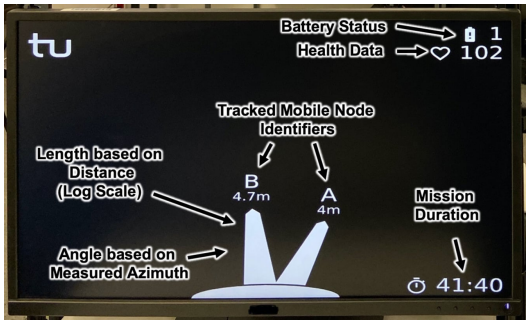

Fig. 6. Functional prototype of the visualization depicted in the heads-up display of the rescue forces. The ad-hoc localization results are depicted next to mission specific information such as battery status, health data and mission duration.

III. Experimental Evaluation

In order to assess the achievable accuracy, three different experiments are conducted. The experiments are conducted in a laboratory environment, equipped with an optical motion capture system with eight cameras that serves as the ground truth as depicted in Fig. 7.

The *CELIDON Cerberus* node, conducting the 3D PDoA and ranging measurements is static at a fixed position. The mobile node, which is based on the same hardware, is equipped with motion capture markers and mounted to a helmet. Due to the height of the helmet-based evaluation and the resulting sub-optimal constellation visible to the motion capture cameras, some outliers are visible in the ground truth measurements. However, these outliers mainly influence the rotation around the yaw axis of the mobile node and are therefore negligible for the assessment of the overall localization capabilities.

In the first experiment the person carrying the mobile node is moving at an almost constant distance in a half-circle trajectory around the node conducting the ad-hoc localization as depicted in Fig. 8. It is clearly visible, that despite small outliers in the elevation angle and larger variances in higher azimuth angles, the proposed approach is capable of tracking the mobile node successfully.

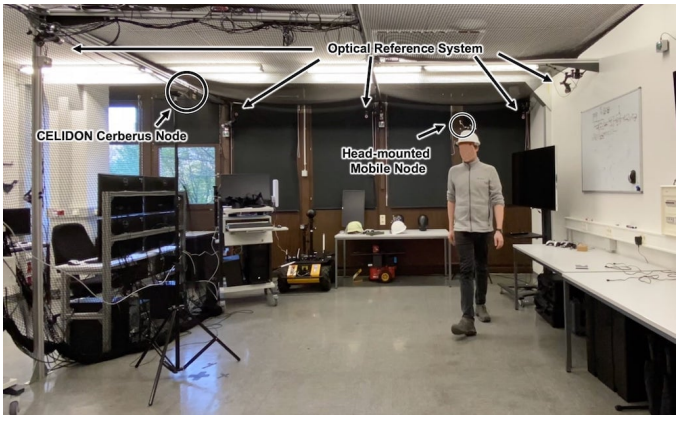

Fig. 7. Annotated picture of the experimental setup. The *CELIDON Cerberus* node is mounted statically on a pole. A mobile node based on the same hardware, but equipped with a single antenna is mounted to a helmet. Ground-truth is provided by an optical reference system.

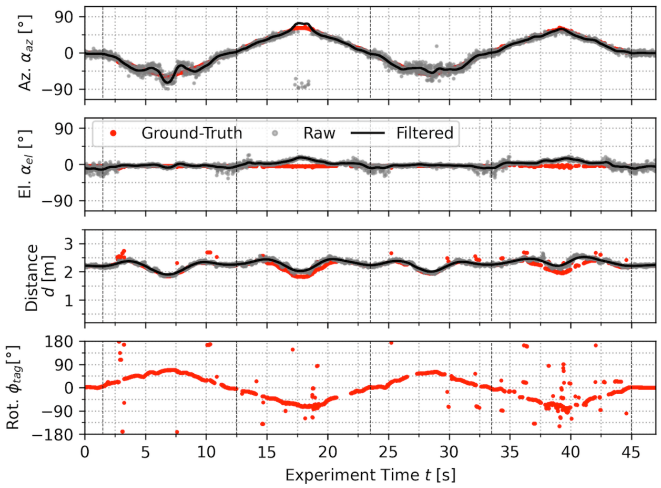

Fig. 8. Timeseries of the experimental results to evaluate the errors in the azimuth angle α_{az}. The raw but compensated readings are depicted next to the filtered measurements and the ground-truth. The rotation ϕ_{tag} of the mobile node (tag) was constantly changed during the experiment such that the front was always facing towards the static node localizing the mobile node.

The second experiment focuses on the variation of the elevation angle. Here, the variation is induced by squatting of the person carrying the mobile node at four different distances as depicted in Fig. 9.

In the third experiment the tag is rotated along the yaw axis along the angle ϕ_{tag} at four different distances as shown in Fig. 10. This is done to evaluate the orientation dependency in practical tracking scenarios. The error of the azimuth and elevation estimation over the rotation of the tag is depicted in Fig. 11. It is clearly visible, that the raw and the filtered

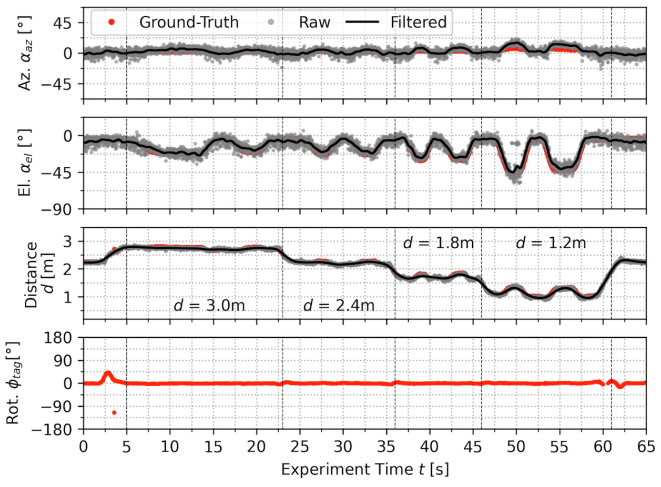

Fig. 9. Timeseries of the experiment focusing on the error in the elevation angle α_{el}. The person carrying the mobile node is squatting at four different distances around a static azimuth angle $\alpha_{az} \approx 0$ and hence, changing the elevation. Note that the rotation ϕ_{tag} of the mobile node (tag) is kept constant.

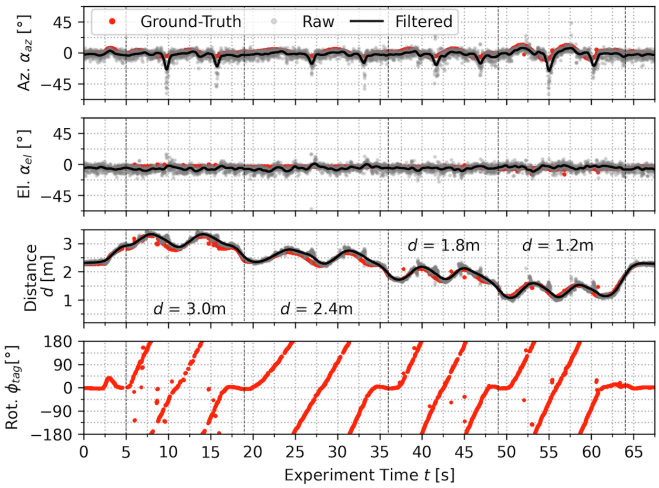

Fig. 10. Timeseries of the experiment to analyze the errors introduced by rotation along the yaw axis ϕ_{tag} of the mobile unit (tag). The oscillation of the distance d is induced by the offset of the antenna to the center of the helmet during rotation. Note the overall good tracking performance in the azimuth and elevation angle.

results are capable of tracking the mobile node well, despite rotation. However, there is a reproducible notch in azimuth around −60°, very likely to be caused by the non-uniform characteristics of the antenna on the mobile node.

The distribution over the full rotation experiment is shown in Fig. 12. This supports the qualitative observations in the timeseries and the plots against the rotation of the mobile node. With the proposed approach tracking in tight error bounds is possible.

In order to assess the overall system performance, the measured values for the azimuth, elevation and distance α_{az}, α_{el} and d are compared against the ground-truth based observations, see Fig. 13. Here, it is clearly visible that an overall good tracking performance can be achieved within the bounds of the experimental analysis. Further, the effects of the filter-approach illustrated in section II-D become visible. This is especially relevant for the elevation angle, where the results could be significantly improved.

In the next step the resulting positioning errors are evaluated. In order to do so, the measured azimuth and elevation angles as well as the distances are converted to relative

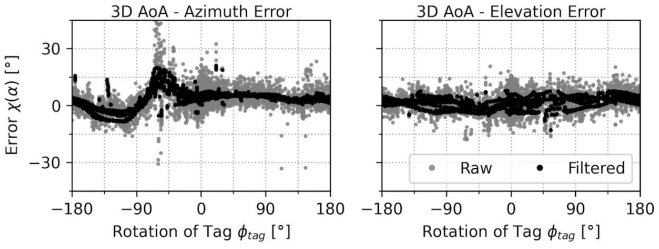

Fig. 11. Plot of the rotation of the tag ϕ_{tag} vs. the error in azimuth (left) and elevation (right) estimation for the eight rotations conducted in this experiment.

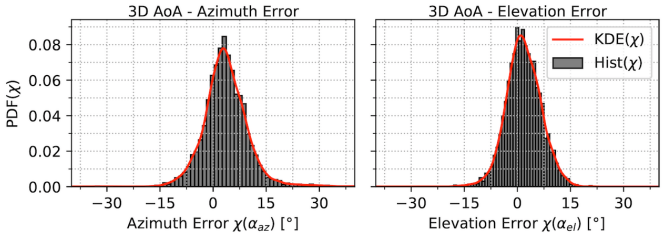

Fig. 12. Distribution in form of a histogram and a kernel density estimation (KDE) of the azimuth and elevation errors for the rotation experiment.

Cartesian coordinates utilizing trigonometric functions. For the evaluation, the two- and three-dimensional euclidean errors where considered. Due to the nature of angle and distance based relative localization, the resulting positioning error will increase with distance. Therefore, the absolute positioning errors achieved within these experiments have to be seen in the context of the laboratory evaluation.

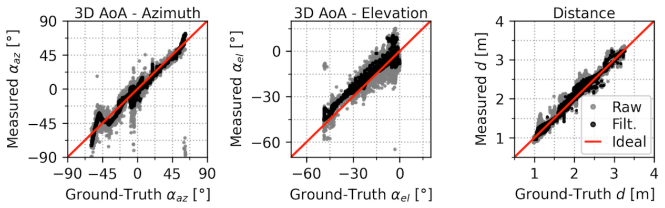

Fig. 13. Correspondence of the measured values in azimuth α_{az} elevation α_{el} and distance d compared to the readings of the ground-truth system.

The resulting cumulative distribution functions (CDF) for the positional errors $|\chi_{(h,p)}|$ and the individual coordinate errors $|\chi_{(x,y,z)}|$ are depicted in Fig. 14. Obviously, the two-dimensional localization is slightly more accurate than the three-dimensional relative position estimation. However, both perform in a similar range, capable of reliable ad-hoc localization. In the third quartile, in 75 % of cases, the localization error of both is below 30 cm for the filtered results. In the 95 % quantile the error is still below 50 cm. The errors within the individual Cartesian components are within a similar range, without major outliers or differences. This illustrates the improvements in comparison to the raw results and show the potential especially for highly reliable localization.

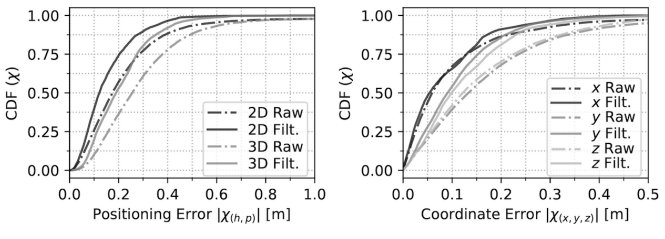

Fig. 14. Cumulative distribution function (CDF) of the resulting positioning errors when utilizing the measurement values to calculate the relative ad-hoc location of the mobile unit.

IV. Conclusion and Future Work

This paper proposes a novel approach to achieve infrastructure-less 3D ad-hoc localization utilizing ultra-wideband (UWB) and phase-difference of arrival (PDoA) estimation to support rescue forces in dangerous operations with low visibility. Due to the highly integrated nature of the hardware developed in the course of this work, integration into equipment of the rescue forces is possible with only minor modification. In an experimental evaluation covering three experiments the achievable performance of the proposed ad-hoc localization could be shown to be more than sufficient to prevent separation by providing a localization accuracy of below 50 cm in 95 % of the considered cases.

In future work large scale experiments in realistic environments are envisioned to validate the performance for use in rescue missions and evaluate the effect of partial non-line of sight operation. Advanced signal assessment and machine-learning approaches are promising candidates to improve reliability in these challenging and complex environments.

Acknowledgment

The work on this paper has been funded by the German Federal Ministry of Education and Research (BMBF) for the project CELIDON (Support of rescue forces through localisation in training and rescue operations) under grant number 13N15011. In the context of this project we would like to thank our partners at the *City of Dortmund, Fire Department Institute of Fire Service and Rescue Technology (IFR)* and the *Westsächsische Hochschule Zwickau, University of Applied Sciences, Chair for Digital Systems* for the good collaboration and their support. Additional partial funding was received through the Deutsche Forschungsgemeinschaft (DFG) within the Collaborative Research Center SFB 876 "Providing Information by Resource-Constrained Analysis", project A4. Further, we would like to thank Manuel Patchou, Florian Schmickmann, Katharina Schweitzer, Thomas Espeter and Julian Withöft for their support. Also, we would like to thank Taoglas for providing early access to the antennas and Decawave for early access on their PDOA design files.

References

[1] R. Mur-Artal and J. D. Tardós. ORB-SLAM2: an open-source SLAM system for monocular, stereo and RGB-D cameras. *IEEE Transactions on Robotics*, 33(5):1255–1262, 2017.

[2] J. Miller, N. Rajagopal, K. K. R. Kumar, A. Luong, and A. Rowe. Realty and reality: Where location matters (using UWB and VIO to localize mobile phones). In *Microsoft Indoor Localization Competition (MILC) as part of the 17th ACM/IEEE International Conference on Information Processing in Sensor Networks (IPSN)*, 2018.

[3] S. Shen, M. Gowda, and R. R. Choudhury. Closing the gaps in inertial motion tracking. In *Proceedings of the 24th Annual International Conference on Mobile Computing and Networking*, MobiCom '18, page 429–444, New York, NY, USA, 2018. Association for Computing Machinery.

[5] G. Schouten and J. Steckel. RadarSLAM: Biomimetic SLAM using ultra-wideband pulse-echo radar. In *2017 International Conference on Indoor Positioning and Indoor Navigation (IPIN)*, pages 1–8, 2017.

[4] J. W. Song and C. G. Park. Enhanced pedestrian navigation based on course angle error estimation using cascaded kalman filters. *Sensors*, 18(4), 2018.

[6] F. Zafari, A. Gkelias, and K. K. Leung. A survey of indoor localization systems and technologies. *IEEE Communications Surveys Tutorials*, 21(3):2568–2599, 2019.

[7] A. Alarifi, A. Al-Salman, M. Alsaleh, A. Alnafessah, S. Al-Hadhrami, M. A. Al-Ammar, and H. S. Al-Khalifa. Ultra wideband indoor positioning technologies: Analysis and recent advances. *Sensors (Basel, Switzerland)*, 16(5):707, May 2016.

[8] D. Lymberopoulos and J. Liu. The microsoft indoor localization competition: Experiences and lessons learned. *IEEE Signal Processing Magazine*, 34(5):125–140, Sep 2017.

[9] F. Potorti, S. Park, A. Ramon J. Ruiz, P. Barsocchi, M. Girolami, A. Crivello, S. Y. Lee, J. H. Lim, J. Torres-Sospedra, F. Seco, R. Montoliu, G. M. Mendoza-Silva, M. D. C. Perez Rubio, C. Losada-Gutierrez, F. Espinosa, and J. Macias-Guarasa. Comparing the performance of indoor localization systems through the EvAAL framework. *Sensors*, 17(10), 2017.

[10] J. Tiemann and C. Wietfeld. Scalability, real-time capabilities and energy efficiency in ultra-wideband localization. *IEEE Transactions on Industrial Informatics*, 2019.

[11] J. Tiemann, Y. Elmasry, L. Koring, and C. Wietfeld. ATLAS FaST: fast and simple scheduled TDOA for reliable ultra-wideband localization. In *IEEE International Conference on Robotics and Automation (ICRA)*, Montréal, Canada, May 2019.

[12] A. Ledergerber and R. D'Andrea. A multi-static radar network with ultra-wideband radio-equipped devices. *Sensors*, 20(6):1599, Mar 2020.

[13] I. Dotlic, A. Connell, H. Ma, J. Clancy, and M. McLaughlin. Angle of arrival estimation using decawave DW1000 integrated circuits. In *2017 14th Workshop on Positioning, Navigation and Communications (WPNC)*, pages 1–6, Oct 2017.

[14] S. Diagne, T. Val, A. K. Farota, B. Diop, and O. Assogba. Performances analysis of a system of localization by angle of arrival UWB radio. *International Journal of Communications, Network and System Sciences*, 13(2):15–27, Feb 2020.

[15] Apple U1 UWB Chip Analysis - TechInsights Report on iPhone 11 Chipsets. https://www.techinsights.com/blog/apple-u1-tmka75-ultra-wideband-uwb-chip-analysis, 2019.

[16] T. Wang, H. Zhao, and Y. Shen. An efficient single-anchor localization method using ultra-wide bandwidth systems. *Applied Sciences*, 10(1):57, Dec 2019.

[17] B. Großwindhager, C. A. Boano, M. Rath, and K. Römer. Concurrent ranging with ultra-wideband radios: From experimental evidence to a practical solution. In *2018 IEEE 38th International Conference on Distributed Computing Systems (ICDCS)*, pages 1460–1467, 2018.

[18] P. Corbalán and G. P. Picco. Ultra-wideband concurrent ranging. *ArXiv, Accepted for publication in the ACM Transactions on Sensor Networks (TOSN)*, abs/2004.06324, 2020.

[19] D. Knobloch. Practical challenges of particle filter based UWB localization in vehicular environments. In *2017 International Conference on Indoor Positioning and Indoor Navigation (IPIN)*, pages 1–5, 2017.

[20] S. Diagne, T. Val, A. Farota, and B. Diop. Comparative analysis of ranging protocols for localization by UWB in outdoor. *Wireless Sensor Network*, 10(5):103–117, May 2018.

[21] IEEE Std 802.15.4z: Task Group 4z Enhanced Impulse Radio. http://www.ieee802.org/15/pub/TG4z.html.

[22] IEEE Std 802.15.4-2015: Part 15.4: Low-Rate Wireless Personal Area Networks (LR-WPANs). http://standards.ieee.org/getieee802/download/802.15.4-2015.pdf.

[23] P. Sedlacek, M. Slanina, and P. Masek. An overview of the IEEE 802.15.4z standard its comparison and to the existing UWB standards. In *2019 29th International Conference Radioelektronika (RADIOELEKTRONIKA)*, pages 1–6, 2019.

[24] R. R. Labbe Jr. Kalman and Bayesian filters in Python. In *Juptyer Notebook based Textbook https://github.com/rlabbe/Kalman-and-Bayesian-Filters-in-Python*, May 2020.